PROCEEDINGS OF SPIE

THz devices based on 2D electron systems

Xing, Huili Grace, Yan, Rusen, Song, Bo, Encomendero, Jimy, Jena, Debdeep

SPIE.

THz Devices Based on 2D Electron Systems

Huili Grace Xing[1,2,3], Rusen Yan,[1] Bo Song,[1] Jimy Encomendero[3] and Debdeep Jena[1,2,3]

[1]School of Electrical & Computer Engineering, Cornell University, Ithaca, NY 14853, USA
[2]Department of Materials Science & Engineering, Cornell University, Ithaca, NY 14853, USA
[3]Department of Electrical Engineering, University of Notre Dame, Notre Dame, IN 46556, USA

*Email: grace.xing@cornell.edu

In two-dimensional electron systems with mobility on the order of $1,000 - 10,000$ cm^2/Vs, the electron scattering time is about 1 ps. For the THz window of $0.3 - 3$ THz, the THz photon energy is in the neighborhood of 1 meV, substantially smaller than the optical phonon energy of solids where these 2D electron systems resides. These properties make the 2D electron systems interesting as a platform to realize THz devices. In this paper, I will review 3 approaches investigated in the past few years in my group toward THz devices. The first approach is the conventional high electron mobility transistor based on GaN toward THz amplifiers. The second approach is to employ the tunable intraband absorption in 2D electron systems to realize THz modulators, where I will use graphene as a model material system. The third approach is to exploit plasma wave in these 2D electron systems that can be coupled with a negative differential conductance element for THz amplifiers/sources/detectors.

1. GaN Based HEMT Devices Towards THz

GaN HEMTs provide a high two-dimensional electron gas (2DEG) density in the order of 10^{13} cm^{-2} due to strong polarization effects and a modest electron mobility up to 2200 cm^2/V·s, which results in an output current density over 4.0 A/mm [1] and in turn a high output power density at a large supply voltage. Moreover, the GaN-on-SiC integration manifests an excellent substrate thermal conduction, which is beneficial to reduce packaging and cooling costs. These features of GaN enable promising power amplifications with high power added efficiency in cellular devices, base stations, wireless networks and defense systems.

Based on the definition of f_T, the frequency when the short circuit current gain h_{21} reaches unity, and the device small signal equivalent circuit analysis (Fig. 1), one can extract an analytical expression for f_T or the total delay time τ_{tot} as a function of equivalent circuit parameters as follows:

$$f_T = \frac{1}{2\pi\tau_{tot}} = \frac{g_m / 2\pi}{(C_{gs} + C_{gd})[1 + (R_s + R_d)/R_{ds}] + g_m C_{gd}(R_s + R_d)}, \tag{1}$$

in which g_m represents the intrinsic transconductance, C_{gs}/C_{gd} the gate-to-source/drain capacitance (the sum of both intrinsic denoted as $C_{gs,int}$ and extrinsic as $C_{gs,ext}$, same for C_{gd}), R_s/R_d the source/drain resistance, and R_{ds} of the channel output resistance. The total delay time τ_{tot} can be further divided into two components: intrinsic delay time τ_{int} and parasitic delay time τ_{par}, expressed as:

$$\tau_{int}=(C_{gs,int}+C_{gd,int})/g_m=L_g/v_e, \tag{2}$$

$$\tau_{par}=(C_{gs,ext}+C_{gd,ext})/g_m+C_{gd}(R_s+R_d)+(C_{gs}+C_{gd})(R_s+R_d)g_{ds}/g_m, \tag{3}$$

in which L_g represents the gate length, and v_e the effective electron velocity.

Fig. 1 Schematic of GaN HEMT structure with small-signal equivalent circuit components.

Fig. 2 (a) Schematic of the InAlN/AlN/GaN HEMT cross section and (b) high resolution (HR) TEM and scanning TEM (inset) images confirming the HEMT layer structures and the 30 nm gate length after device fabrication [2], (c) Small-signal RF characteristics of the HEMT with L_g=30 nm [reproduced from Ref.9] and (d) the evolution of f_T in the last one decade for both III-V pHEMTs and GaN HEMTs [reproduced from Ref.10].

To improve the device speed, the first intuitive way is to reduce the τ_{int} by scaling down the gate length thus the intrinsic capacitance assuming a constant v_e/g_m. The gate-length scaling in GaN HEMTs, not different much from Si CMOS and III-V pHEMTs scaling, can be further pushed by adopting resist reflow and/or dielectric-assisted lithography technology with high throughput after reaching the physical lithography limit. In our group, a gate length as short as 30-nm was achieved, shown in Fig. 2(b) [2]; without an effective back barrier, further reduction in L_g will not lead to a faster transistor. A 20-nm-long footprint with AlGaN back barrier has been successfully demonstrated using a dielectric sidewall process by HRL [3], which is the shortest gate length ever reported in GaN HEMTs. With decananometer L_g, the parasitic delay can reach 30-50% of the total delay. Therefore, it is equally important to minimize parasitics by reducing the parasitic resistances, including the ohmic contact resistance R_c and S/D access resistances R_{as}/R_{ad} and extrinsic capacitance $C_{gs,ext}/C_{gd,ext}$ as shown in Fig 1. Regrown ohmic contacts by MBE have been developed to address the contact resistance with ultra-low contact resistance lower than 0.1 Ω.mm [2-4]. To suppress R_{as} and R_{ad}, a low sheet resistance R_{sh} enabled by InAlGaN/AlN barriers, such as a record low 129 Ω/sq in AlN HEMTs [5], and/or ultra-scaled S/G and D/G distances [3,6] are highly desired. Ultra-thin passivation, e.g. dielectric free passivation by the plasma process [7], also is introduced to minimize the extrinsic capacitance. With respect to R_{ds}, a vertical top barrier thickness t_{bar} scaling plus a better carrier confinement with back barriers, e.g. AlN/GaN/AlN quantum-well HEMTs represent one of the best solutions in mitigating short channel effects (SCEs) [8], and consequently increase R_{ds}. Combined the aforementioned

advanced technologies, InAlN HEMTs with a rectangular gate length of 30-nm and regrowth ohmic have shown record f_T up to 400 GHz shown in Fig. 2 [9] and comparison with the state-of-the-art high speed device in GaN based device and other III-V HEMT [10].

With the continual scaling in both L_g and L_{ds} down to sub-100nm regime and optimization of the parasitic, the devices speed is limited by the parasitic delay, ultimately by the first term of Eq.1 associated with the extrinsic capacitance $(C_{gs,ext}+C_{gd,ext})$ and g_m [11]. The extrinsic capacitance, dependent on the device geometry and passivation (both thickness and dielectric constant), would not scale down with L_g. Shown in Fig.3(a) and (b), the extrinsic capacitance exhibits weak dependence on gate recess, while the intrinsic capacitance and g_m scale inversely with the remaining recessed barrier thickness. This means that the intrinsic delay is independent of recess depth while the parasitic delay decreases with the reducing remaining barrier thickness since g_m increases. Thus, the device speed increases with more aggressive gate recess, provided the v_{eff} is not affected by the recess etch. It is $(C_{gs,ext}+C_{gd,ext})/g_m$ that defines the ultimate speed limit after both L_g and R_{on} scale down to zero in theory. Therefore, maximizing g_m is key to obtaining terahertz transistors. This is consistent with the observation that InGaAs-channel HEMTs exhibit higher speed than GaN or Si based FETs. To further improve the GaN HEMT speed, it is paramount to seek approaches that enhance injection velocity thus $g_{m,int}$, such as the use of InGaN [12] or isotope-disordered channels [13].
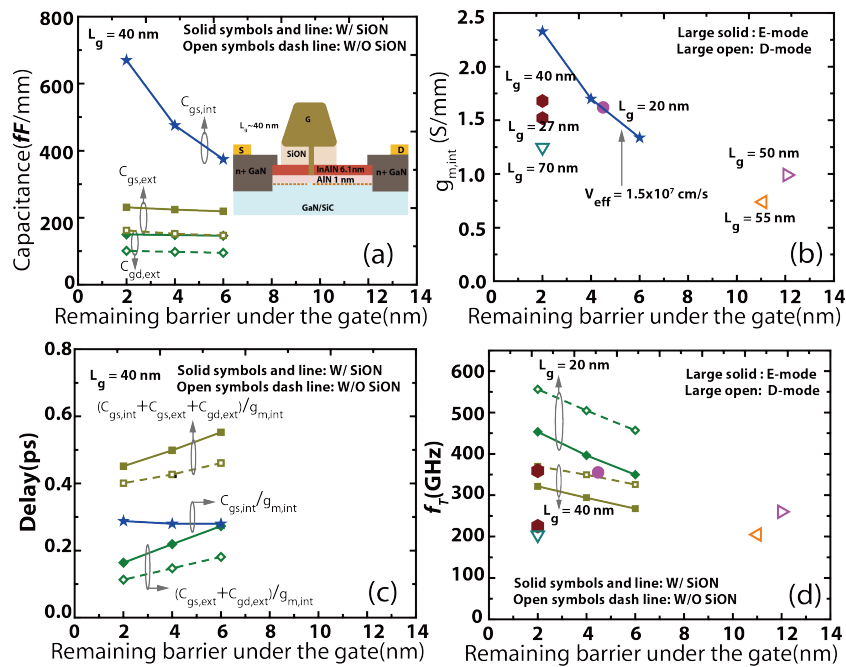
Fig. 3 Calculated performance of GaN HEMTs with a gate stem height of 200 nm, recessed gate and a thin barrier shown in the insert of Fig (a). For a gate length of 40 nm, (a) extrinsic and intrinsic capacitances, (b) estimated intrinsic gm and reported values, and (c) delays. The intrinsic delay stays the same (SCEs neglected), the extrinsic delay decreases purely because of the enhancement in gm. (d) Projected fT for devices with Rs/Rd of 0.11/0.18 Ω.mm and two gate lengths: 20 and 40 nm. Also shown are $g_{m,int}$ and f_T values of several reported high performance E-mode GaN HEMTs with T-gate and f_T > 200 GHz (large solid symbols) [reproduced from Ref.10].

Aggressive gate length scaling and optimization of GaN HEMT has led to impressive progress reaching device speed about 400 GHz. The extrinsic delay is found to be a significant factor in limiting the speed in ultra-scaled GaN HEMTs, and is fundamentally determined by the device

intrinsic g_m and the fringing capacitance between the gate stem and the access regions. Thus improving g_m by enhancing injection velocity with further gate-length scaling is key in realizing GaN THz devices.

2. Graphene Based THz Modulators

The awarding of Nobel Prize in 2010 acquaints the world with graphene. As a single sheet of carbon atoms arranged in hexagonal structure, graphene possesses unique physical properties that are hardly seen in traditional semiconductors, which stimulates tremendous amount of interests in both scientists and engineers [14-18]. Thanks to the significant progress in large-area mass production of graphene by chemical vapor deposition (CVD) [19-21] in recent years, the applications of graphene have been expanded to a variety of aspects. The very unique combination of high electric conductivity and optical transparency makes graphene an appropriate candidate for transparent conducting electrodes. Comparing to the commercial indium-tin-oxide (ITO), graphene is much more favorable considering its excellent mechanical strength, tenability, flexibility, low-price and facile integration. Technologies such as touch screen, solar cells, light-emitting diodes, liquid crystal displays etc all have the needs of transparent electrodes which can be replaced by graphene. In this work, we demonstrate one novel function of graphene as transparent electrode in internal photoemission spectroscopy (IPE) for the first time [22-24].
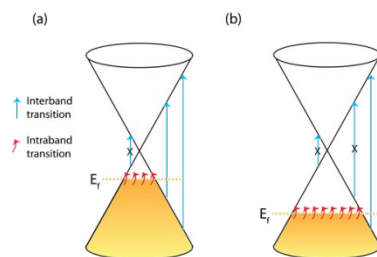
Fig. 4 (a) and (b) Band diagrams of graphene with two different Fermi levels showing the interband (blue arrow) and intraband (red arrow) transitions. In THz range, intraband transition dominates due to the small photon energy required. As Fermi level goes further from Dirac point ((a) to (b)), states of free carriers available for intraband transition increases.

However, that's not the whole story. Recently, our group showed the terahertz (THz) wave transmission through the graphene layer can be electrically tuned by varying its Fermi levels [25-27]. It is amazing that a layer of carbon atoms with the thickness 1000,000 times smaller the wavelength can so efficiently modulate the electromagnetic waves. In visible range, graphene exhibits flat transmission spectrum of 97%, which is almost independent its Fermi levels [28]. On the contrary, in THz range, intra-band carrier transition dominates due to the low incident photon energy, resulting in a Fermi level dependent transmittance [29,30]. As shown in Fig. 4, the available states that could induce THz absorption is larger while the Fermi level stays further from the Dirac point. Therefore, such intraband absorption based THz modulation could be readily realized by tuning graphene's Fermi level with various approaches. Previously, several types of modulators in THz range have been proposed and demonstrated. For example, HEMT-like device with a 2DEG layer between GaAs/AlGaAs interface could modulate THz transmission by 3% by tuning the electron density [31]. Another strategy is to apply metamaterials to concentrate waves into a doped GaAs layer [32, 33]. By depleting carriers in GaAs beneath the split gap of metallic structure by applying biases, THz transmission is enhanced due to the less absorption by free carriers. In addition, MEMS-based reconfigurable mesh filters are recently explored [34]. Despite the superior modulation depth (>70%), the operation speed is rather slow (20 KHz) hindered by the mechanical control of the system. In

comparison, graphene based THz modulation possess advantages of large modulation depth, high speed, and facile fabrication procedure [35].

As the first experimentally demonstrated graphene-based THz modulator, our proof-of-concept device employs a graphene-SiO_2-Si structure as shown in Fig. 5, to tune the THz wave transmission by applying a voltage between the top contact and the back gate metal [25]. A 1.5 x 1.5 cm^2 monolayer graphene layer grown by CVD on Cu foil was transferred onto a 300 nm SiO_2 covered Si substrate. To avoid the free carrier loss induced by the substrate, a lightly doped p-type Si wafer is used. Then top and backside contacts were deposited by e-beam evaporation. Figure 5a shows the DC conductivity (blue circles) and the detector response (green squares) at 600 GHz, where it could be clearly seen that transmission increases with decreasing DC electrical conductivity as expected. Because the Dirac voltage is ≥ 50, so it could be inferred that the graphene is p-type in all the range of scanned gate voltage from 0 to 50V. The transmission spectrum at two gate voltage values after removing the substrate oscillation effects is shown in Fig. 5b. The flat transmission characteristic of this modulator promises the intrinsically broadband operation. Modulation depth (MD) defined as $(T_{max}-T_{min})/T_{max}$ could be calculated to be 15±2% over the entire spectrum.
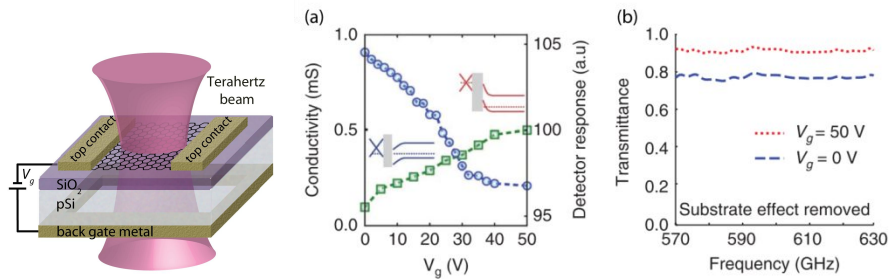

Fig. 5 The structure of electro-absorption THz modulator which consists of a graphene on SiO_2 covered p-type Si substrate. The THz beam is normal incidence to the structure. (a) Measured DC conductivity (blue circles) and detector response (green squares) at 600 GHz as a function of gate voltages. The insets respectively show the band diagrams of graphene-SiO_2-Si structure when the gate voltage is 0 V and 50 V. (b) Measured transmission intensity after removing the substrate and free carrier absorption in lightly doped Si substrate under two gate voltages. All figures are reproduced from Ref. 25.
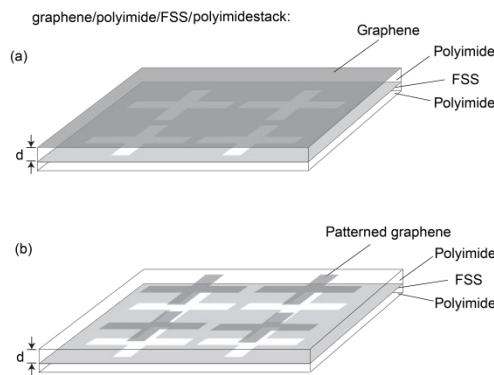

Fig. 6 Schematic of the device structure with (a) un-patterned and (b) patterned graphene layers.

The promising performance of this prototype graphene modulator opened up a way for future THz devices. However, limited by the conductivity swing of typical quality of the state-of-the-art large-area graphene, such designs still cannot ensure practical applications. Following this demand, we have proposed and experimentally demonstrated that by taking advantage of the

enhanced field in the near field of metallic frequency selective surface (FSS), exceptional MD can potentially be achieved in graphene-based THz modulators [36]. It is found that, the distance between graphene layers and FSS can modify the strength of graphene-THz photon interaction, thus, by placing graphene layers at an optimal distance away from FSS, an improved electro-absorption modulation for THz waves can be obtained. More importantly, due to the highly spatially localized electromagnetic field in the near field of the FSS, we show that the modulator MD and IL can be maintained when the graphene is patterned into the complementary structure of the FSS. As a result, the substantial reduction of graphene area can enable high operation speed of THz modulators. Here by stacking and pattering 1-3 layers of graphene, we are able to tune the graphene conductivity from 0.8 mS to 2.4 mS, corresponding to a 65% intensity modulation. The thin-film flexible samples are fabricated on a polyimide (PI) substrate as schematically shown in Fig. 6a and b, consisting of graphene separated from the FSS by a polyimide spacer with a variable thickness.

(a)

(b)
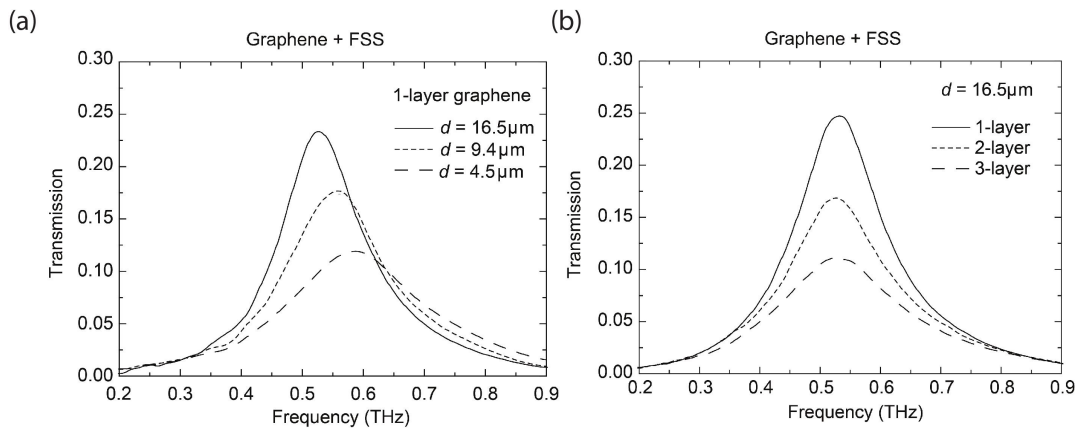
Fig. 7 (a) THz intensity transmission through the structure described in Fig. 6a with spacer thickness of 16.5 μm, 9.4 μm, 4.5μm. (b) THz intensity transmission through the structure described in Fig. 6a with 1-, 2-, and 3- layer of graphene respectively.
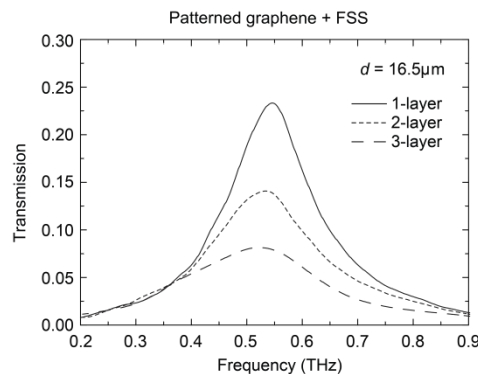
Fig. 8 THz intensity transmission through the structure described in Fig. 6(b) with 1-, 2-, and 3- layer of patterned graphene respectively.

To investigate the effects of distance d between graphene and metallic FSS, we measured the power transmittance of the sample with 1-layer graphene but various spacer thickness $d = 16.5$ μm, 9.4 μm, 4.5 μm. It could be seen that for graphene layer with similar conductivity (all of them is around 0.8 mS), THz transmission at resonant frequency gradually decreases when graphene is placed closer to FSS due to the stronger near-field effects [36]. As graphene gets

closer to FSS, the direction of poynting vector below FSS tends to be more in-plane to the graphene layers, which corresponds to stronger interaction between graphene and THz waves, resulting in lowered THz transmission through the sample. Besides, the resonant frequency shifts due to the change of effective capacitance with varied sample thickness. The measured THz transmission through fabricated structure with 1-3 graphene layers as absorption medium but same spacer thickness d = 16.5 μm is shown in Fig. 7. Note that the extracted total conductivity of 1-, 2- and 3-layer graphene layers is respectively 0.7 mS, 1.3 mS, and 2.0 mS, approximately equal to the sum of the conductivities of the individual graphene layers [37]. As conductivity increases, THz transmission drops. Simulations processed in HFSS match well with measured transmission values, demonstrating the potential of THz intensity tuning in proposed structures [36].

More importantly, we found that, transmission of THz waves through the entire structure maintains after patterning graphene layers into complementary structure of the FSS. We proceeded to fabricating sample structure as shown in Fig. 6b with 1-3 layers of graphene transferred and patterned into the shape of cross slot. The THz transmission is then measured in THz TDS and shown in Fig. 8. Interestingly, we notice that the power transmitted through the structures covered by patterned graphene is similar to that of samples with un-patterned graphene layers. These observations are also confirmed by HFSS simulations using the conductivity values extracted from Drude mode fitting, where the sum of graphene conductivities for 1-, 2- and 3-layers can be determined to be about 0.8 mS, 1.6 mS, and 2.4 mS. Considering the fact that almost all the THz electromagnectic waves at resonant frequency have to travel through the opening area in the FSS, the waves are highly spatially confined inside the shape of cross slots. Therefore, the graphene area complimentary to FSS is primarily responsible for wave intensity absorption, which is the reason why patterned graphene based structure layers can show similar transmissions as un-patterned ones. It is known that, one of fundamental issues limiting the operation speed of graphene-based THz modulators is the large resistance and capacitance induced active area of graphene films [25]. Our finding here is remarkably advantageous for future THz modulators by reducing the un-patterned graphene area to patterned structures but still maintaining the similar modulation strength.

3. Plasma-Waves in 2D Electron systems

Two-dimensional (2D) electron systems formed in the channel of sub-micrometer transistors enable the propagation of electron-density oscillations for frequencies laying in the THz region of the spectrum. These so-called plasma waves are generated when individual electrons in the channel are not able to follow high frequency oscillations and lag behind. The delay exhibited by the electrons presents an inductive behavior, which in turn couples with the gate-channel capacitor to give rise to a resonator of electron-density waves. The dynamics of these waves and their non-linear effects can be exploited to realize detectors, mixers and multipliers for frequencies inside the THz band [38]. In particular, resonant THz detectors have been demonstrated up to 3.1 THz for a 50-nm-InGaAs-channel-based high electron mobility transistor (HEMT) [39]. More recently, an asymmetric dual grating gate (A-DGG) was introduced by Watanabe et al. which harness the non-linear effects of 2D plasma waves and enhances detector responsivity with respect to the symmetric dual grating gate (S-DGG) layout [40]. This approach was employed to demonstrate highly sensitive THz detectors with responsivities up to 6.4kV/W at 1.5THz [41] and 22.7kV/W at 200GHz [42], operating in the non-resonant regime. The successful development of THz detectors makes plasma-wave electronics a good candidate for leveraging the THz band of the spectrum and this approach can be used for the fabrication of active THz devices with amplification and signal generation capabilities.

The predicted trends in performance for different device concepts in the THz band, including plasmonic field effect transistors (FETs), are displayed in Fig. 9 in terms of output power and

frequencies of operation [43]. Devices based on inter-sub-band transitions such as quantum cascade lasers (QCL) present also a promising trend towards the generation of THz signals. In this sense, III-N based quantum cascade structures are considered as good candidates for the fabrication of compact solid-state sources of THz radiation in contrast to the traditional III-V materials, which are incapable of emitting radiation around their LO-phonon energies (~34 meV ~8.2 THz for InGaAs) [44].
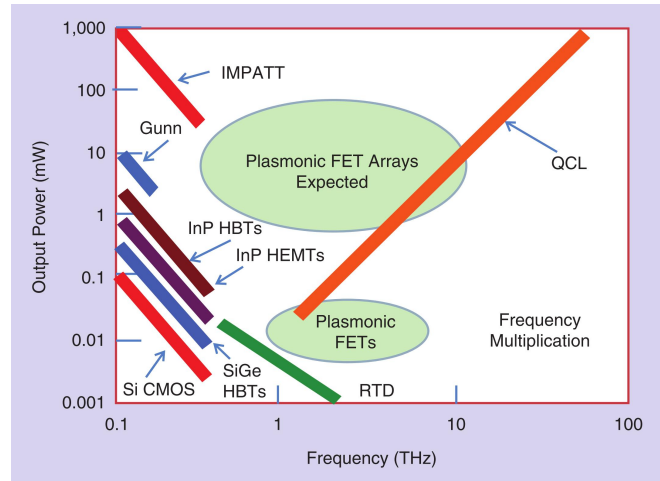
Fig. 9 Predicted trends in performance for different device concepts, including plasmonic field effect transistors (FETs) and quantum cascade lasers (QCLs). Plasmonic FET arrays can be also considered as an approach to increase the output power of THz signals [43].

A second approach to enhance non-resonant THz detection was proposed by studying the effect of gate leakage in the plasma oscillations inside the channel [45]. The gate current leakage limits the amplitude of the electron-density oscillations thus degrading the responsivity of the device. The opposite effect can be achieved if the differential conductance between the gate and the channel is negative. This negative differential conductance (NDC) can be engineered if a tunneling double barrier structure is epitaxially grown on top of the channel.

In addition to enhancing the responsivity of a plasma-wave detector, the NDC also acts as a gain medium, which can not only prevent the density oscillations from damping but also amplify its swing [46]. The dynamics of a gated 2D electron gas (2DEG) formed in the channel of a plasma-wave HEMT can be modeled by a distributed transmission line scheme [47]. This scheme is also used to model the frequency response of the resonant tunneling diode gated plasma wave HEMT (RTD-gated-plasma wave HEMT). Figure 10 shows the distributed circuit model for an RTD-gated plasma wave HEMT including the 2DEG kinetic inductance l, the 2DEG resistance r, the resonant tunneling capacitance c_i, and the NDC g_i. It should be noted that the distributed scheme also takes into account the variation of the voltage in the channel V_{ch_i} and every single of the "lumped" element is a function of the non-uniform bias along the channel as well as the non-uniform 2DEG from the source to the drain, namely plasma wave.

The design of a THz RTD-gated plasma wave HEMT, using the InGaAs-material system as an example has shown that power amplification larger ~10 dB is possible at ~3 THz for a 190 nm-channel [48]. The voltage gain vs. frequency is displayed in Fig. 11; amplification and higher harmonic generation of THz signals evidence the gain provided the RTD gate and the non-linear nature of plasma-waves respectively.
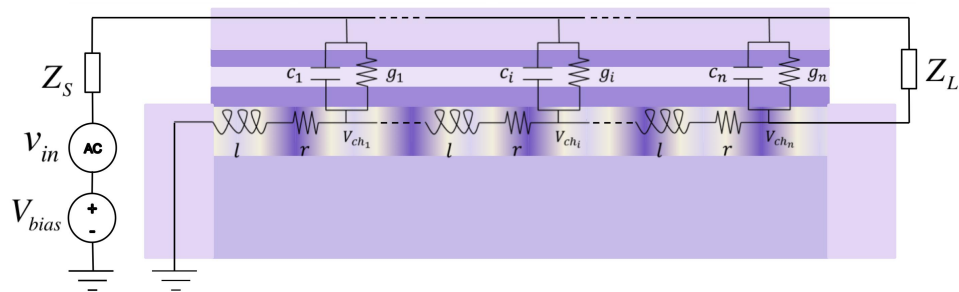
Fig. 10 Distributed high frequency transmission line model for a resonant tunneling diode gated plasma wave high electron mobility transistor (RTD-gated plasma wave HEMT). The tunneling double barrier provides the negative differential conductance (NDC), which in turn allows for the amplification of the plasma-waves in the channel.
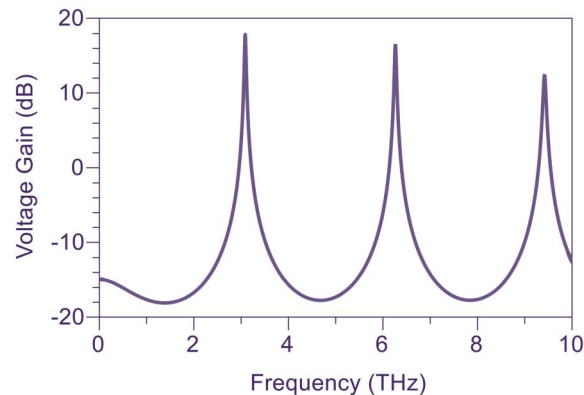
Fig. 11 Voltage gain vs. frequency for an InGaAs-based RTD-gated plasma wave HEMT [48]. Amplification and higher harmonic generation of THz signals evidence the gain provided the RTD gate and non-linear behavior of the 2D electron-density oscillations.

Wide band-gap materials such as GaN are also attractive for power amplification of THz signals. In this sense, recent investigations have successfully measured the kinetic inductance of the 2DEG at frequencies in the G-band (140-220 GHz) [49]. A good agreement was found between the measured and the kinetic inductance predicted by the distributed transmission line model; showing conclusively that plasma-oscillations were exited in the channel. These results show that the realization of plasma wave devices with the advantage of high power and high frequency capabilities are feasible.

The emerging plasma wave electronic devices exhibit promising trends towards the creation of THz sources and amplifiers. High power scalability can be provided by wide band-gap materials or by using arrays of plasmonic devices as can be seen in Fig.9. Finally, electronics based on electron-density oscillation also have the advantage of tunable operation and high-speed modulation of THz waves which can be employed in a variety of applications [50].

REFERENCES

[1] K. Shinohara, D. Regan, A. Corrion, D. Brown, Y. Tang, J. Wong, G. Candia, A. Schmitz, H. Fung, S. Kim and M. Micovic, "Self-Aligned-Gate GaN-HEMTs with Heavily-Doped n+-GaN Ohmic Contacts to 2DEG," in IEDM Tech. Dig. pp. 27.2, 2012.

[2] Y. Yue, Z. Hu, J. Guo, B. Sensale-Rodriguez, G. Li, R. Wang, F. Faria, T. Fang, B. Song, X. Gao, S. Guo, T. Kosel, G. Snider, P. Fay, D. Jena and H. Xing, "InAlN/AlN/GaN HEMTs With Regrown Ohmic Contacts and f(T) of 370 GHz," IEEE Elec. Dev. Lett., vol. 33, pp. 988-990, JUL 2012. 2012.

[3] K. Shinohara, D. Regan, A. Corrion, D. Brown, S. Burnham, P.J. Willadsen, I. Alvarado-Rodriguez, M. Cunningham, C. Butler, A. Schmitz, S. Kim, B. Holden, D. Chang, V. Lee, A. Ohoka, P.M. Asbeck and M. Micovic, "Deeply-Scaled Self-Aligned-Gate GaN DH-HEMTs with Ultrahigh Cutoff Frequency," in IEDM Tech. Dig. pp. 19.1, 2011.

[4] J. Guo, G. Li, F. Faria, Y. Cao, R. Wang, J. Verma, X. Gao, S. Guo, E. Beam, A. Ketterson, M. Schuette, P. Saunier, M. Wistey, D. Jena and H. Xing, "MBE-Regrown Ohmics in InAlN HEMTs With a Regrowth Interface Resistance of 0.05 Omega . mm," IEEE Elec. Dev. Lett., vol. 33, pp. 525-527, APR 2012.

[5] Y. Cao, K. Wang, G. Li, T. Kosel, H. Xing, and D. Jena, "MBE growth of high conductivity single and multiple AlN/GaN heterojunctions," J. Crys. Growth, vol. 323, pp. 529-533, 2011

[6] S.D. Nidhi, D.F. Brown, S. Keller, J.S. Speck and U.K. Mishra, "N-polar GaN-based highly scaled self-aligned MIS-HEMTs with state-of-the-art f(T).L-G product of 16.8 GHz-mu m," in IEDM Tech. Dig. pp. 464-466, 2009.

[7] R. Wang, G. Li, O. Laboutin, Y. Cao, W. Johnson, G. Snider, P. Fay, D. Jena, and H. Xing, "210-GHz InAlN/GaN HEMTs with dielectric-free passivation," IEEE Electron Device Lett., vol. 32, no. 7, pp. 892-894, Jul. 2011.

[8] G. Li, R. Wang, J. Guo, J. Verma, Z. Hu, Y. Yue, F. Faria,Y. Cao, M. Kelly, T. Kosel, H. G. Xing, and D. Jena, "Ultra-thin body GaN-on-insulator quantum well FETs with regrown ohmic contacts," IEEE Electron Device Lett., vol. 33, no. 5, pp. 661–663, May 2013

[9] Y. Yue, Z. Hu, J. Guo, B. Sensale-Rodriguez, G. Li, R. Wang, F. Faria, T. Fang, B. Song, X. Gao, S. Guo, T. Kosel, G. Snider, P. Fay, D. Jena, H. Xing "Ultrascaled InAlN/GaN High Electron Mobility Transistors with Cutoff Frequency of 400 GHz, " Jpn. J. Appl. Phys, vol. 52, no. 8, pp. 08JN14-1 - 08JN14-2, Aug. 2013 2012.

[10] R.Wang, " InAl(Ga)N-Barrier GaN HEMTS FOR High Speed Applications," Ph. D. Disertation, Univ. of Notre Dame, 2012.

[11] B. Song, B. Sensale-Rodriguez, R. Wang, J. Guo, Z. Hu, Y. Yue, F. Faria, M. Schuette, A. Ketterson, E. Beam, P. Saunier, X. Gao, S. Guo, P. Fay, D. Jena, H.G.Xing, "Effect of Fringing Capacitances on the RF Performance of GaN HEMTs With T-Gates," IEEE Trans Elec. Dev.,, vol.61, no.3, pp.747-754, March 2014

[12] R.Wang,G. Li, G. Karbasian, J. Guo, F. Faria, Z. Hu, Y. Yue, J. Verma,O. Laboutin, Y. Cao, W. Johnson, G. Snider, P. Fay, D. Jena, and H. Xing, "InGaN channel high-electron-mobility transistors with InAlGaN barrier and f_T /f_{max} of 260/220 GHz," Appl. Phys. Exp., vol. 6, no. 1,pp. 016503-1 - 016503-3, Jan. 2013.

[13] J.B. Khurgin, D. Jena, Y. Ding, "Isotope disorder of phonons in GaN and its beneficial effect on high power field effect transistors, " Appl. Phys. Lett. , vol.93, no.3, pp.032110-1- 032110-3, Jul 2008.

[14] H. Castro Neto, N. M. R. Peres, K. S. Novoselov, and a. K. Geim, "The electronic properties of graphene," Rev. Mod. Phys., vol. 81, no. 1, pp. 109–162, Jan. 2009.

[15] K. Geim and K. S. Novoselov, "The rise of graphene.," Nat. Mater., vol. 6, no. 3, pp. 183–91, Mar. 2007.

[16] K. S. Novoselov, a K. Geim, S. V Morozov, D. Jiang, Y. Zhang, S. V Dubonos, I. V Grigorieva, and a a Firsov, "Electric field effect in atomically thin carbon films.," Science, vol. 306, no. 5696, pp. 666–9, Oct. 2004.

[17] K. S. Novoselov, A. K. Geim, S. V Morozov, D. Jiang, M. I. Katsnelson, I. V Grigorieva, S. V Dubonos, and A. A. Firsov, "Two-dimensional gas of massless Dirac fermions in graphene.," Nature, vol. 438, no. 7065, pp. 197–200, Nov. 2005.

[18] Y. Zhang, T.-T. Tang, C. Girit, Z. Hao, M. C. Martin, A. Zettl, M. F. Crommie, Y. R. Shen, and F. Wang, "Direct observation of a widely tunable bandgap in bilayer graphene," Nature, vol. 459, no. 7248, pp. 820–823, Jun. 2009.

[19] K. S. Kim, Y. Zhao, H. Jang, S. Y. Lee, J. M. Kim, K. S. Kim, J.-H. Ahn, P. Kim, J.-Y. Choi, and B. H. Hong, "Large-scale pattern growth of graphene films for stretchable transparent electrodes," Nature, vol. 457, no. 7230, pp. 706–710, Feb. 2009.

[20] X. Li, W. Cai, J. An, S. Kim, J. Nah, D. Yang, R. Piner, A. Velamakanni, I. Jung, E. Tutuc, S. K. Banerjee, L. Colombo, and R. S. Ruoff, "Large-Area Synthesis of High-Quality and Uniform Graphene Films on Copper Foils," Sci. , vol. 324 , no. 5932 , pp. 1312–1314, Jun. 2009.

[21] C. Mattevi, H. Kim, and M. Chhowalla, "A review of chemical vapour deposition of graphene on copper," J. Mater. Chem., vol. 21, no. 10, p. 3324, 2011.

[22] R. Yan, Q. Zhang, W. Li, I. Calizo, T. Shen, C. a. Richter, A. R. Hight-Walker, X. Liang, A. Seabaugh, D. Jena, H. Grace Xing, D. J. Gundlach, and N. V. Nguyen, "Determination of graphene work function and graphene-insulator-semiconductor band alignment by internal photoemission spectroscopy," Appl. Phys. Lett., vol. 101, no. 2, p. 022105, 2012.

[23] R. Yan, Q. Zhang, O. A. Kirillov, W. Li, J. Basham, A. Boosalis, X. Liang, D. Jena, C. A. Richter, and A. C. Seabaugh, "Graphene as transparent electrode for direct observation of hole photoemission from silicon to oxide," Appl. Phys. Lett., vol. 102, no. 12, p. 123106, 2013.

[24] K. Xu, C. Zeng, Q. Zhang, R. Yan, P. Ye, K. Wang, A. C. Seabaugh, H. G. Xing, J. S. Suehle, C. a Richter, D. J. Gundlach, and N. V Nguyen, "Direct measurement of Dirac point energy at the graphene/oxide interface.," Nano Lett., vol. 13, no. 1, pp. 131–6, Jan. 2013.

[25] B. Sensale-Rodriguez, R. Yan, M. M. Kelly, T. Fang, K. Tahy, W. S. Hwang, D. Jena, L. Liu, and H. G. Xing, "Broadband graphene terahertz modulators enabled by intraband transitions.," Nat. Commun., vol. 3, p. 780, Jan. 2012.

[26] B. Sensale-Rodriguez, R. Yan, S. Rafique, M. Zhu, W. Li, X. Liang, D. Gundlach, V. Protasenko, M. M. Kelly, D. Jena, L. Liu, and H. G. Xing, "Extraordinary control of terahertz beam reflectance in graphene electro-absorption modulators.," Nano Lett., vol. 12, no. 9, pp. 4518–22, Sep. 2012.

[27] B. Sensale-Rodriguez, T. Fang, R. Yan, M. M. Kelly, D. Jena, L. Liu, and H. (Grace) Xing, "Unique prospects for graphene-based terahertz modulators," Appl. Phys. Lett., vol. 99, no. 11, p. 113104, 2011.

[28] R. R. Nair, P. Blake, A. N. Grigorenko, K. S. Novoselov, T. J. Booth, T. Stauber, N. M. R. Peres, and A. K. Geim, "Fine Structure Constant Defines Visual Transparency of Graphene," Sci. , vol. 320 , no. 5881 , p. 1308, Jun. 2008.

[29] T. Stauber, N. Peres, and a. Geim, "Optical conductivity of graphene in the visible region of the spectrum," Phys. Rev. B, vol. 78, no. 8, p. 085432, Aug. 2008.

[30] L. a Falkovsky, "Optical properties of graphene," J. Phys. Conf. Ser., vol. 129, p. 012004, Oct. 2008.

[31] T. Kleine-Ostmann, P. Dawson, K. Pierz, G. Hein, and M. Koch, "Room-temperature operation of an electrically driven terahertz modulator," Appl. Phys. Lett., vol. 84, no. 18, pp. 3555–3557, May 2004.

[32] H.-T. Chen, W. J. Padilla, J. M. O. Zide, A. C. Gossard, A. J. Taylor, and R. D. Averitt, "Active terahertz metamaterial devices.," Nature, vol. 444, no. 7119, pp. 597–600, Nov. 2006.

[33] H.-T. Chen, W. J. Padilla, M. J. Cich, A. K. Azad, R. D. Averitt, and A. J. Taylor, "A metamaterial solid-state terahertz phase modulator," Nat Phot., vol. 3, no. 3, pp. 148–151, Mar. 2009.

[34] C. W. Berry, J. Moore, and M. Jarrahi, "Design of reconfigurable metallic slits for terahertz beam modulation," Opt. Express, vol. 19, no. 2, pp. 1236–1245, Jan. 2011.

[35] B. Sensale-Rodriguez, R. Yan, L. Liu, D. Jena, and H. G. Xing, "Graphene for Reconfigurable Terahertz Optoelectronics," Proc. IEEE, vol. 101, no. 7, pp. 1705–1716, Jul. 2013.

[36] R. Yan, B. Sensale-Rodriguez, L. Liu, D. Jena, and H. G. Xing, "A new class of electrically tunable metamaterial terahertz modulators.," Opt. Express, vol. 20, no. 27, pp. 28664–71, Dec. 2012.

[37] H. Yan, F. Xia, W. Zhu, M. Freitag, C. Dimitrakopoulos, A. A. Bol, G. Tulevski, and P. Avouris, "Infrared Spectroscopy of Wafer-Scale Graphene", ACS Nano 2011 5 (12), 9854-9860.

[38] Dyakonov, M., and Shur, M., "Detection, mixing and frequency multiplication of terahertz radiation by two-dimensional electronic fluid," IEEE Trans. Electron Devices, vol. 43, pp. 380-387 (1996).

[39] El Fatimy, A. and Teppe, F. and Dyakonova, N. and Knap, W. and Seliuta, D. and Valušis, G. and Shchepetov, A. and Roelens, Y. and Bollaert, S. and Cappy, A. and Rumyantsev, S., "Resonant and voltage-tunable terahertz detection in InGaAs∕InP nanometer transistors" Applied Physics Letters, 89, 131926 (2006).

[40] Takayuki Watanabe, Stephane Boubanga Tombet, Yudai Tanimoto, Yuye Wang, Hiroaki Minamide, Hiromasa Ito, Denis Fateev, Viacheslav Popov, Dominique Coquillat, Wojciech Knap, Yahya Meziani, Taiichi Otsuji, "Ultrahigh sensitive plasmonic terahertz detector based on an asymmetric dual-grating gate HEMT structure", Solid-State Electronics 78 109-114 (2012).

[41] Boubanga-Tombet, S.; Tanimoto, Y.; Watanabe, T.; Suemitsu, T.; Yuye, W.; Minamide, H.; Ito, H.; Popov, V.; Otsuji, T., "Asymmetric dual-grating gate InGaAs/InAlAs/InP HEMTs for ultrafast and ultrahigh sensitive terahertz detection," Device Research Conference (DRC), 2012 70th Annual , vol., no., pp.169,170, 18-20 June 2012.

[42] Kurita, Y. and Ducournau, G. and Coquillat, D. and Satou, A. and Kobayashi, K. and Boubanga Tombet, S. and Meziani, Y. M. and Popov, V. V. and Knap, W. and Suemitsu, T. and Otsuji, T., "Ultrahigh sensitive sub-terahertz detection by InP-based asymmetric dual-grating-gate high-electron-mobility transistors and their broadband characteristics" Applied Physics Letters, 104, 251114 (2014).

[43] Otsuji, T.; Shur, M., "Terahertz Plasmonics: Good Results and Great Expectations," Microwave Magazine, IEEE , vol.15, no.7, pp.43,50, Nov.-Dec. 2014.

[44] Jovanović, V. D. and Indjin, D. and Ikonić, Z. and Harrison, P., "Simulation and design of GaN/AlGaN far-infrared (λ∼34 μm) quantum-cascade laser" Applied Physics Letters, 84, 2995-2997 (2004).

[45] B. Sensale-Rodríguez, P. Fay, L. Liu, D. Jena, H. G. Xing, "Enhanced Terahertz Detection in Resonant Tunnel Diode-Gated HEM "ECS Trans. 2012 Vol. 49, issue 1, 93-102.

[46] B. Sensale-Rodríguez, L. Liu, P. Fay, D. Jena, H. G. Xing, "Power Amplification at THz via Plasma Wave Excitation in RTD-Gated HEMT " IEEE Transactions on Terahertz Science and Technology 3, 200-206 (2013).

[47] P. J. Burke, I. B. Spielman, J. P. Eisenstein, L. N. Pfeiffer, K. W. West, "High frequency conductivity of the high-mobility two-dimensional electron gas" Appl. Phys. Lett. 76, 745 (2000).

[48] Jimy J. Encomendero-Risco, Berardi Sensale-Rodriguez, Patrick Fay, Grace Xing, "RTD-gated HEMT non-linear circuit model for THz amplification", LEC Conference 2014.

[49] Zhao, Y. and Chen, W. and Li, W. and Zhu, M. and Yue, Y. and Song, B. and Encomendero, J. and Sensale-Rodriguez, B. and Xing, H. and Fay, P., "Direct electrical observation of plasma wave-related effects in GaN-based two-dimensional electron gases" Applied Physics Letters, 105, 173508 (2014).

[50] V.Yu. Kachorovskii, M.S. Shur, 'Field effect transistor as ultrafast detector of modulated terahertz radiation, Solid-State Electronics', Volume 52, Issue 2, February 2008, Pages 182-185.